# High temperature hydrothermal alteration and amphibole formation in Gakkel Ridge abyssal peridotites

Sierra N. Patterson, Kendra J. Lynn, Cécile Prigent, Jessica M. Warren

Lithos 392–393 (2021) 106107

Contents lists available at ScienceDirect

Lithos

journal homepage: www.elsevier.com/locate/lithos

Research Article

# High temperature hydrothermal alteration and amphibole formation in Gakkel Ridge abyssal peridotites

Sierra N. Patterson *,[1], Kendra J. Lynn [2], Cécile Prigent [3], Jessica M. Warren

*Department of Earth Sciences, University of Delaware, 255 Academy Street, Newark, DE 19716, USA*

ARTICLE INFO

*Article history:*
Received 15 August 2020
Received in revised form 21 February 2021
Accepted 5 March 2021
Available online 16 March 2021

*Keywords:*
Hydrothermal alteration
Abyssal peridotite
Gakkel Ridge
Amphibole

ABSTRACT

Alteration mineral assemblages in abyssal peridotites offer insights into the temperature and pressure conditions during hydrothermal fluid circulation in the oceanic lithosphere. Abundant hydrothermal venting has been documented along the ultraslow spreading Gakkel Ridge and peridotites have been extensively sampled from the ridge, yet these peridotites have not been systematically evaluated for the nature and extent of their alteration. Here, we present an analysis of the alteration of 40 Gakkel peridotites from 19 dredges spanning ~600 km of the ridge within the Sparsely Magmatic and Eastern Volcanic Zones. We use a petrographic-based alteration scoring system to assign a rank to each sample of 1 (unaltered) to 5 (altered) in 0.5 step intervals, based on the alteration scale of Birner et al. (2016). Gakkel peridotites cover the full range of alteration, from essentially unaltered to completely serpentinized, but are generally moderately to highly altered (average score of 3.5). The extent of alteration is independent of peridotite lithology and is not systematically different between the two zones. Serpentine is present in all samples, magnetite occurs in all samples with alteration scores >2.5, and 27% of samples contain carbonate veins that cross-cut all other minerals. In 20% of samples, all with alteration scores >2.5, tremolite + talc occurs as rims around pyroxene, while chlorite occurs as haloes around spinel. A gabbro-veined lherzolite also contains pargasite replacing pyroxene, with later overprinting by tremolite-talc intergrowths.

The abundance of tremolite, chlorite, and talc in Gakkel samples is much lower than reported for talc-tremolite-chlorite schists from oceanic core complexes, where fluid flow through the lower crust leads to open-system behavior. At Gakkel, our petrological observations suggest that alteration was nearer to closed-system conditions, which can be explained by the absence of crust along some sections of the ridge. Pseudosection modeling with Perple_X, which assumes closed-system behavior, indicates that pyroxene reacts to form tremolite + chlorite + talc at temperatures >500 °C, corresponding to fluid flow to depths >20 km for the Gakkel Ridge. The sample with pargasitic amphibole requires temperatures >750 °C to form. Overall, our results suggest that hydrothermal alteration of Gakkel peridotites, and more generally of the lithospheric mantle in regions that lack significant crust, results in different alteration mineral abundances and relationships than in regions where the mafic crust is involved in alteration.



## 1. Introduction

Abyssal peridotites are ultramafic mantle samples that are exposed on the seafloor at mid-ocean ridges, transform faults, and subduction zones. The circulation of hydrothermal fluids through cracks in the lithospheric mantle results in mineral replacement reactions, with deeper fluid circulation leading to increasingly higher temperature reactions. The conditions (temperature, pressure, fluid composition) of hydrothermal processes can be evaluated from the alteration mineral assemblages that form at the expense of the primary mineral assemblage of olivine + pyroxenes + spinel ± plagioclase. At temperatures <500 °C, serpentine, brucite, and magnetite are produced from the reaction of aqueous fluids with olivine and pyroxene (e.g., Allen and Seyfried, 2003; Bach et al., 2004; Klein et al., 2009, 2015; Tutolo et al., 2018). Between 300 and 500 °C, pyroxene reacts with water to form other alteration phases such as tremolite, chlorite, and talc (e.g., Bach et al., 2004; Früh-Green et al., 2004; Jenkins, 1981; Schmidt and Poli, 1998). At temperatures of 800–1000 °C, alteration of peridotites results in the crystallization of higher temperature minerals such as amphibole with pargasite and Mg-hornblende compositions (Fumagalli et al., 2009).

Most work on hydrothermal alteration of mid-ocean ridge peridotites has focused on samples that are either close to oceanic core complexes (e.g., Boschi et al., 2006a; Früh-Green et al., 2004; Morishita

* Corresponding author.
*E-mail address:* sierranp@seoe.sc.edu (S.N. Patterson).
[1] now at University of South Carolina.
[2] now at U.S. Geological Survey.
[3] now at Institut de Physique du Globe de Paris.

https://doi.org/10.1016/j.lithos.2021.106107

et al., 2009) or transform faults (e.g., Bach et al., 2004; Früh-Green et al., 2001; Kimball et al., 1985). In these regions, mafic crust (gabbros and basalts) is usually present and involved in the hydrothermal alteration reactions. Recently, Rouméjon et al. (2015) and Dessimoulie et al. (2020) characterized serpentinization processes in mantle rocks from a magma-poor region along a corridor orthogonal to the ultraslow spreading Southwest Indian Ridge (SWIR). However, the nature and extent of alteration beyond serpentinization reactions has yet to be evaluated in detail for any long section of peridotite exposure along a mid-ocean ridge.

The Gakkel Ridge in the Arctic Ocean is ideal for characterizing the alteration history of mantle rocks because peridotites have been dredged from many locations along this ultraslow spreading ridge, especially from the central Sparsely Magmatic Zone (SMZ; Michael et al., 2003). Additionally, active hydrothermal circulation is indicated by the identification of 9–12 vent sites based on water column measurements and near-bottom imaging (Edmonds et al., 2003; Helmke et al., 2007; Stranne et al., 2010; Boetius et al., 2014; Bünz et al., 2020). These sites occur primarily in association with volcanic centers, but at least one is associated with ultramafic rocks (Edmonds et al., 2003).

Here we evaluate the extent, nature, and conditions of aqueous fluid-rock interaction in peridotites from a ~ 600 km long section of the Gakkel Ridge. While some Gakkel peridotites exhibit minor degrees of serpentinization, most samples have undergone intense hydrothermal alteration and many contain a variety of alteration minerals. Our results provide some of the first systematic observations of alteration mineralogy along a peridotite-dominated section of ridge and suggest that alteration can reach relatively high temperatures, even in ultraslow spreading environments.

## 2. Geological setting

The Gakkel Ridge is the northernmost and slowest spreading mid-ocean ridge on Earth (Fig. 1). Its spreading rate decreases by a factor of two from west to east along strike, with a full spreading rate as low as 6.3 mm/year (DeMets et al., 1994). Contrary to expectations that volcanism is diminished at ultraslow spreading rates, the Gakkel Ridge is one of the few places globally where both basalts and peridotites are exposed over hundreds of kilometers along the ridge axis (Michael et al., 2003). The ridge has been divided into three major magmato-tectonic zones (Fig. 1) that are characterized by differing degrees of volcanic activity and relative abundances of rock types: the Western Volcanic Zone (WVZ), Sparsely Magmatic Zone (SMZ) and the Eastern Volcanic Zone (EVZ).

As peridotites were not dredged from the WVZ, this study focuses on samples from the SMZ and EVZ. While basalts are present in the SMZ, volcanic ridges are absent and peridotites dominate the lithology of recovered material. The EVZ is the slowest-spreading section of Gakkel, yet is punctuated by six large volcanic centers. Five dredges returned peridotites from an otherwise basalt-dominated section of the ridge (Michael et al., 2003).

In this study, we focus on 15 dredges from the SMZ (~270 km length) and 4 dredges from the EVZ (>350 km length), corresponding to samples from ~600 km of ridge length (Fig. 1; Supplementary Table S1). Peridotite lithologies from the SMZ and the EVZ range from relatively fertile lherzolites to refractory harzburgites (D'Errico et al., 2016). As shown in Fig. 1, evidence for hydrothermal venting has been identified in the water column at one SMZ and four EVZ locations within our study region (Edmonds et al., 2003). Dredges with the closest proximity to a hydrothermal plume signal are EVZ dredges HLY0102–70, −85 and − 87, and SMZ dredge PS59–240 (Fig. 1). Two SMZ dredges (HLY0102–40 and PS59–235) contain unusually fresh peridotite (D'Errico et al., 2016; von der Handt, 2008) and are not located near any recorded plume signal (Fig. 1).

## 3. Methodology

### 3.1. Petrographic analyses and alteration scores

We conducted petrographic analysis of 40 peridotite samples from 19 dredges to classify the level of alteration and associated alteration mineral assemblages (Table 1). Fourteen of these samples were previously

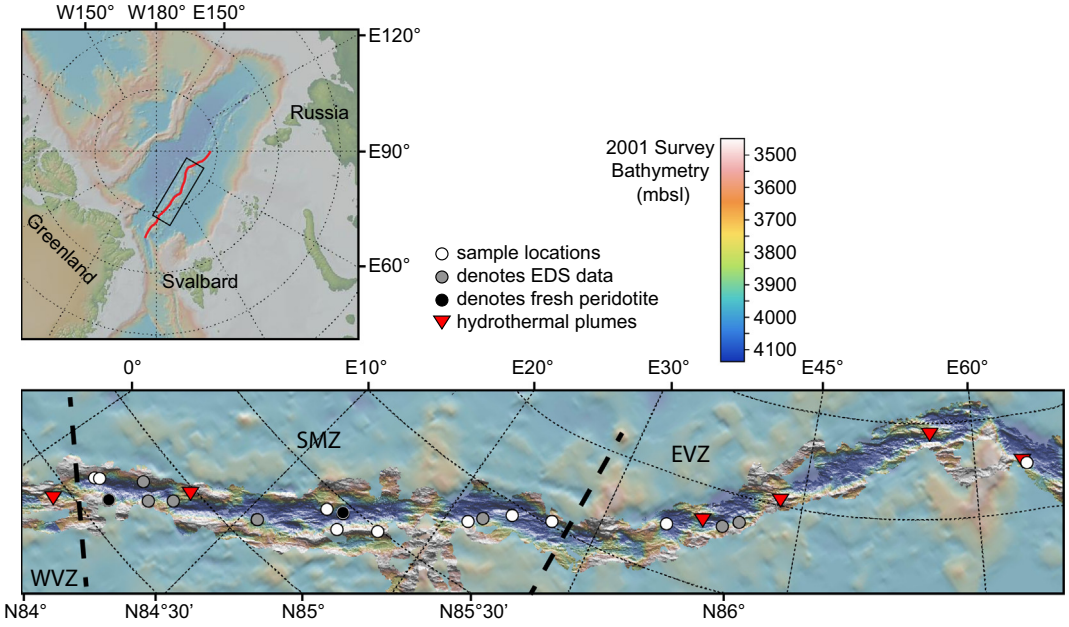


**Fig. 1.** Bathymetric map of the Gakkel Ridge with a north polar projection showing the location of the 19 studied dredges (circles), including dredges that recovered unusually fresh peridotites (black circles) and our focus samples that we characterized by EDS (gray circles). The locations of hydrothermal plume sites (red triangles) are from Edmonds et al. (2003). Thick dashed lines separate the Western Volcanic Zone (WVZ), Sparsely Magmatic Zone (SMZ), and Eastern Volcanic Zone (EVZ). Bathymetric maps were generated using GeoMapApp (Ryan et al., 2009) with 100 m resolution bathymetry from the AMORE 2001 cruise (Michael et al., 2003).

**Table 1**
Lithology and alteration scores and mineralogy for Gakkel Ridge abyssal peridotites.

| Sample no. | Lithology | Rank | Tr | Chl | Tlc | Cb |
|---|---|---|---|---|---|---|
| HLY102–0443 | Harzburgite | 4.5 | X | X | X | |
| HLY102–04-63* | Plag Lherzolite | 3.5 | | | | X |
| HLY102–29-21 | Lherzolite | 3 | | | | |
| HLY102–30-01 | Lherzolite | 4.5 | | | | |
| HLY102–39-01 | Harzburgite | 4 | | | | |
| HLY102–39-02 | Harzburgite | 5 | | | | |
| HLY102–40-18 | Refractory Harzburgite | 3 | | | | X |
| HLY102–40-56 | Refractory Harzburgite | 1.5 | | | | |
| HLY102–40-79 | Refractory Harzburgite | 2 | | | | |
| HLY102–40-81 | Refractory Harzburgite | 1.5 | | | | |
| HLY102–70-62 | Harzburgite | 3.5 | | | | |
| HLY102–70-75 | Lherzolite | 4 | | | | |
| HLY102–70-87 | Plag Lherzolite | 3 | X | X | | |
| HLY102–70-91 | Lherzolite | 3.5 | | | | |
| HLY102–85-09* | Harzburgite | 4 | X | | | X |
| HLY102–87-32* | Lherzolite | 3 | X | X | X | X |
| HLY102–87-37 | Harzburgite | 4 | X | X | X | X |
| HLY102–92-36 | Lherzolite | 4 | | | | |
| HLY102–100-13 | Lherzolite | 3.5 | | | | X |
| HLY102–100-80 | Harzburgite | 3.5 | | | | |
| PS59–201-39 | Refractory Harzburgite | 3.5 | | | | X |
| PS59–201-40 | Refractory Harzburgite | 4 | | | | X |
| PS59–235-01 | Lherzolite | 2 | | | | |
| PS59–235-04 | Plag Websterite | 1 | | | | |
| PS59–235-17 | Lherzolite | 1.5 | | | | |
| PS59–235-18 | Lherzolite | 2 | | | | |
| PS59–238-59* | Harzburgite | 4.5 | | | | X |
| PS59–238-75 | Lherzolite | 3 | X | X | X | |
| PS59–240-20* | Lherz + Gabbro Vein | 3 | X | X | X | X |
| PS59–240-21 | Harzburgite | 5 | | | | |
| PS59–240-36 | Plag Harzburgite | 4.5 | | | | |
| PS59–246-01* | Harzburgite | 4 | X | X | X | |
| PS59–246-03 | Refractory Harzburgite | 4.5 | X | | | |
| PS59–249-12 | Harzburgite | 3.5 | X | | | X |
| PS59–249-60 | Refractory Harzburgite | 3 | X | | | X |
| PS59–249-74* | Refractory Harzburgite | 3.5 | X | X | X | |
| PS59–257-07 | Harzburgite | 4.5 | X | X | X | |
| PS59–257-15 | Harzburgite | 3.5 | | | | |
| PS59–317-06 | Harzburgite | 4.5 | | | | |
| PS59–318-50 | Plag Harzburgite | 4.5 | | | | |

Note(s):
Samples with an asterisk are focus samples described in more detail in Table 2.
Abbreviations: Tr = tremolite; Chl = chlorite; Tlc = talc; Cb = carbonate.
All samples have serpentine, with rank providing a proxy for degree of serpentinization.

characterized by D'Errico et al. (2016) for their primary mineralogy and mantle melting history. Peridotite lithologies consist of 11 lherzolites, 14 harzburgites, 9 refractory harzburgites (<1% clinopyroxene and < 1 wt% $Al_2O_3$) and six plagioclase-bearing samples (Table 1).

Petrographic analysis was conducted using a Leica 2500P microscope to determine Gakkel peridotite mineralogy and alteration score, from 1 to 5 in 0.5 step increments (Table 1) based on the qualitative alteration scale from Birner et al. (2016). This scale mainly classifies the degree of hydrothermal alteration based on the level of serpentinization. A score of 1 indicates unaltered peridotite with essentially no alteration minerals, while 5 indicates completely altered peridotite with no primary minerals remaining except for spinel (Fig. 2). Some samples contain zones with different levels of alteration, in which case alteration assignments are based on the freshest portion of the sample. While this is an underrepresentation of the full extent of hydrothermal alteration, the original purpose of the scale was to evaluate samples suitable for analysis of their primary mineralogy (Birner et al., 2016).

Forearc peridotites exposed in the Pacific Tonga Trench ($n = 41$) from the Birner et al. (2016) study were evaluated alongside the Gakkel samples. As Tonga is the only other region where the alteration scale has been applied, the re-analysis of Tonga samples was used to (1) confirm that the scale was being correctly applied in this study and (2) evaluate the uncertainty of this method. In evaluating Tonga peridotites, we reassigned alteration scores of 12 Tonga samples by either ± half step compared to the values from Birner et al. (2016). The average in Tonga alteration scores between Birner et al. (2016) and this study are nearly identical (Supplementary Table S2), indicating that the uncertainty related to subjective determination of sample scores is small.

### 3.2. SEM-EDS analyses

Seven samples (Table 2) were selected for additional analysis using a scanning electron microscope (SEM) with an energy dispersive X-ray spectroscopy (EDS) detector. EDS maps and point analyses were collected using an Oxford Instruments X-Max 80 $mm^2$ silicon drift detector attached to a Zeiss Auriga 60 Crossbeam SEM at the W. M. Keck Center for Advanced Microscopy and Microanalysis at the University of Delaware. The SEM field emission gun was operated at an accelerating voltage of 15–20 kV and an aperture of 30 μm. Data were processed using Aztec v3.4 software.

### 3.3. Whole rock analyses

We obtained whole rock major element data for a subset of eight samples in this study along with six Tonga samples (Supplementary Table S3). These were combined with previously collected data for Gakkel and Tonga samples (Birner et al., 2017; Craddock et al., 2013) to evaluate compositional range as a function of alteration score. We prepared rock chips for crushing by cutting off exterior surfaces and ultrasonicating in deionized water for up to one hour to remove loose particles. Following the previous studies, whole rock powders were prepared and analyzed by the Washington State University GeoAnalytical Laboratory (Johnson et al., 1999).

### 3.4. Pseudosections

Using whole rock data, pseudosections were built to constrain the pressure (P) - temperature (T) - fluid conditions at which observed alteration mineral assemblages are stable and hydrothermal processes took place. Our pseudosection modeling assumes closed-system hydrothermal alteration, where hydration of peridotites only results in addition of water to their initial chemistry. Modeling was performed using

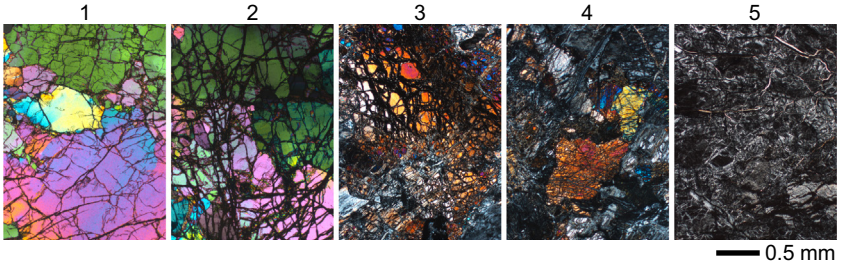


**Fig. 2.** Photomicrographs in cross polarized light of Gakkel Ridge peridotite samples representative of the hydrothermal alteration scale of 1 to 5 developed by Birner et al. (2016).

**Table 2**
Alteration mineralogy of Gakkel focus samples[a]

| Sample no. | Lithology | Alt. Rank | Ank | Cb | Chl | Crn | Ilm | Mag | Prg | Srp | Tlc | Tr |
|---|---|---|---|---|---|---|---|---|---|---|---|---|
| HLY102–04-63 | Pl-Lherzolite | 3.5 | | X | | | | X | | X | | |
| HLY102–85-09 | Harzburgite | 4 | X | X | | X | | X | | X | | X |
| HLY102–87-32 | Lherzolite | 3 | | | X | | | X | | X | X | X |
| PS59–238-59 | Harzburgite | 4.5 | | X | | | | X | | X | | |
| PS59–240-20 | Lherz + Gabbro Vein | 3 | | X | X | | X | X | X | X | X | X |
| PS59–246-01 | Harzburgite | 4 | | | X | | | X | | X | X | X |
| PS59–249-74 | Refractory Harzburgite | 3.5 | | | X | | | X | | X | X | X |

Note(s): Mineral abbreviations: (Ank) = ankerite, (Cb) = carbonate, (Chl) = chlorite, (Crn) = corundum, (Ilm) = ilmenite, (Mag) = magnetite, (Prg) = pargasite, (Srp) = serpentine, (Tlc) = talc, (Tr) = tremolite.
[a] All samples contain relicts of the primary mineral assemblage Ol + Opx + Cpx + Spl ± Pl.

Perple_X software (Connolly, 2009) in the NCFMASH ($Na_2O$-CaO-FeO-MgO-$Al_2O_3$-$SiO_2$-$H_2O$) chemical system, using the same thermodynamic solid solution models as those reported in Prigent et al. (2020). Pseudosections were calculated for water-saturated condition. A lower water content changes the abundance but not the stability of hydrous phases (Prigent et al., 2020).

We used the compositional extremes of peridotite samples with fresh alteration scores of 1–2 to model alteration reactions occurring in peridotites affected by variable degrees of partial melting. Samples BMRG08–98–2-1 (alteration score = 1, Tonga Trench) and PS59–235-17 (alteration score = 1.5, Gakkel Ridge) respectively define the refractory harzburgite and fertile lherzolite end-member compositions. For the lherzolite pseudosection, Na-phlogopite or nepheline appear at conditions where high-T amphibole (pargasite) is not stable. These phases were removed as they are not observed in any of our samples.

To evaluate the change in mantle mineralogy with depth during alteration, we required a P-T path through the Gakkel lithosphere. The geotherm at the Gakkel Ridge has not been modeled in detail. However, seismic data indicate that the maximum depth of microearthquakes is at ~35 km depth at the SMZ and oscillates between ~15 and 30 km depth in the WVZ and EVZ (Schlindwein and Schmid, 2016). This depth represents the brittle-ductile transition of peridotites, which correspond to the ~600–700 °C isotherm (Abercrombie and Ekström, 2001; Engeln et al., 1986; Wiens and Stein, 1983). Using these constraints, we modeled the Gakkel Ridge geotherm assuming a linear P-T path starting at seafloor conditions and passing through a depth limit for Gakkel seismicity of 30 km (10 kbar) at ~700 °C (Schlindwein et al., 2015). The modal percentage of phases at thermodynamic equilibrium was then calculated along this P-T path.

## 4. Results

### 4.1. Gakkel peridotite alteration scores

The full range (from 1 to 5 on the alteration scale) of hydrothermal alteration is present among the 40 peridotite samples evaluated from 19 Gakkel dredges (Table 1). The degree of alteration does not vary systematically between lherzolites and harzburgites. Gakkel peridotites have an average alteration score of 3.5 ± 1, which is higher than Tonga peridotites (2.9 ± 1), as shown in Fig. 3. While alteration scores of Tonga peridotites are almost evenly distributed (sub-linear cumulative frequency curve), only a small number (18%) of Gakkel peridotites have a score ≤ 2, while 43% of Gakkel samples have a score ≥ 4 (Fig. 3). Two out of 19 Gakkel dredges (HLY0102–40 and PS59–235), compared to six out of 14 Tonga dredges (Supplementary Table S2 of Birner et al., 2016), contain samples categorized with an alteration score ≤ 2.5.

### 4.2. Petrographic and EDS constraints on alteration mineralogy

The primary mineral assemblage of most Gakkel peridotites consists of olivine, clinopyroxene, orthopyroxene, and spinel (Fig. 2). Six

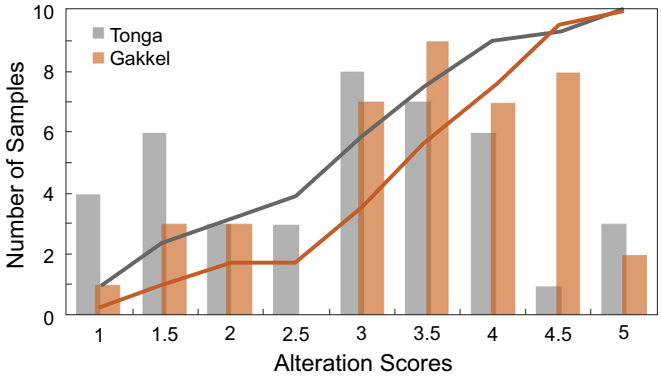


**Fig. 3.** Comparison of Gakkel Ridge and Tonga Trench peridotite alteration scores. Tonga peridotite scores (Supplementary Table S2) use the values determined in this study, which was used to test analyst subjectivity in assigning a score. These values are identical for 29 samples and different by ±0.5 for 12 samples compared to the original scores from Birner et al. (2016). Gray and orange lines are the cumulative frequency distributions for Tonga and Gakkel, respectively.

samples also contain plagioclase (Table 1), often identifiable in hand sample as altered white patches, but only two samples, PS59–235-04 and PS59–240-20, contain fresh plagioclase in thin section. Sulfides occur in Gakkel peridotites as a trace primary phase (e.g., D'Errico et al., 2019) and as an alteration phase. We did not evaluate the systematics of sulfide alteration due to their low modal abundance.

All samples contain serpentine, ranging from very minor amounts in fresh samples (alteration score ≤ 2) to multiple generations of cross-cutting veins in the highly altered samples (Fig. 2). For samples with alteration scores ≤2, serpentine ± magnetite is the only alteration phase, occurring as incipient serpentinization on fractures and grain boundaries. Of the 33 samples with alteration scores ≥3, fifteen samples (45%) have only serpentine and magnetite as alteration phases, based on petrographic analysis. Many of these samples have a variety of serpentine crystallization textures and multiple generations of cross-cutting serpentine veins, similar to those described by Andreani et al. (2007) and Rouméjon et al. (2015).

Tremolitic amphibole (Fig. 4a) was identified in 33% of samples and occurs only in peridotites with alteration scores ≥3 (Table 1). Sample lithology is independent of tremolite occurrence as it occurs in both harzburgites and lherzolites. Tremolite predominantly occurs in alteration rims and cracks in orthopyroxene, while clinopyroxene is less often altered to tremolite (Supplementary Fig. S1). In some samples, tremolite was found in cross-cutting veins (Fig. 5a) and as patches in the serpentine matrix (Supplementary Fig. S2). Tremolite also occurs as intergrowths with serpentine and with cross-cutting serpentine veins, indicating that tremolite formation occurred prior to, during and after serpentinization.

Chlorite (Fig. 4b) is present in nine peridotites, all of which are tremolite-bearing (Table 1). Chlorite was most typically found as

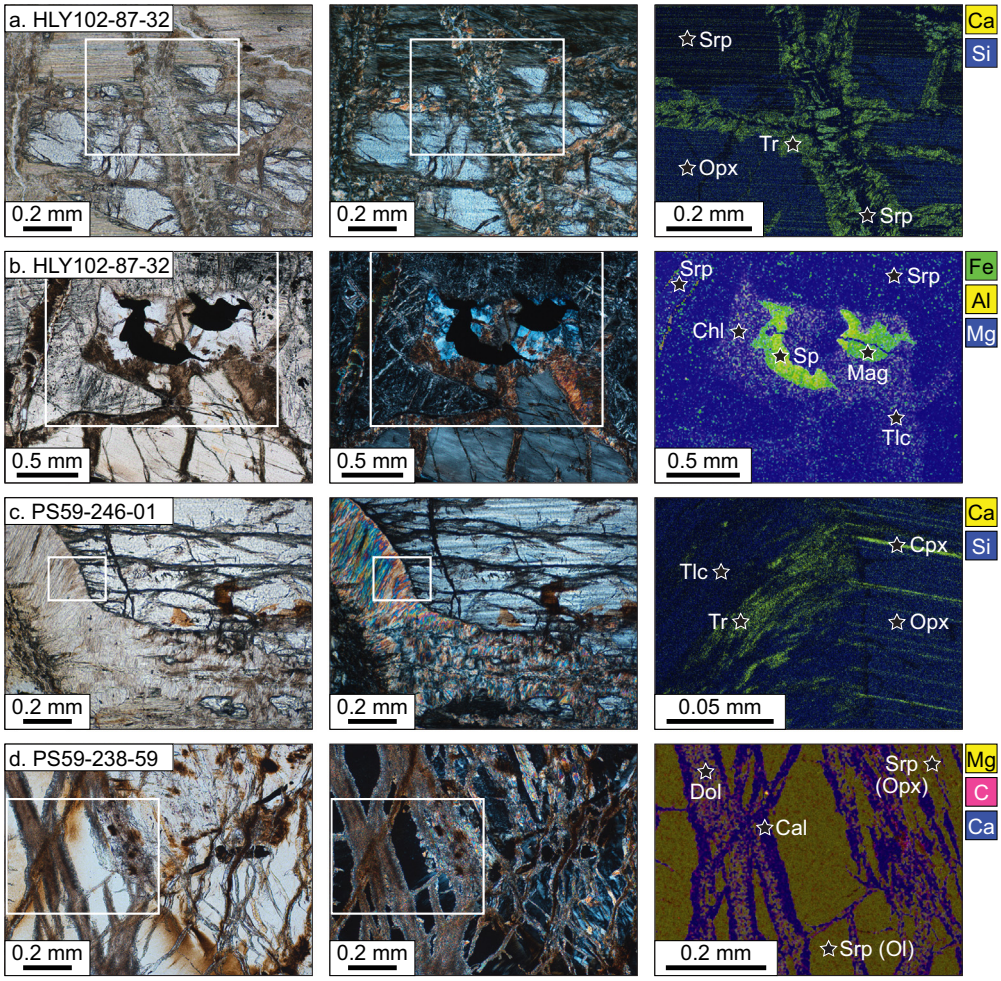


**Fig. 4.** Examples of alteration phases that are common in Gakkel peridotites. Plane-polarized photomicrographs are in column 1, cross-polarized photomicrographs in column 2, and EDS maps in column 3. White boxes indicate the location of the EDS maps. (a) Tremolite-filled alteration cracks in partially serpentinized orthopyroxene (HLY102–87-32). (b) Chlorite haloes around spinel, which is partially altered to magnetite. Surrounding material is mesh-texture serpentine + magnetite and a serpentine bastite pseudomorph of orthopyroxene (HLY102–87-32). (c) Alteration rim on orthopyroxene, consisting of tremolite and talc (PS59–246-01). (d) Carbonate mesh network of veins overprinting mesh-texture serpentine that has replaced olivine and bastite-texture serpentine that has pseudomorphed orthopyroxene. (PS59–238-59). Mineral abbreviations: (Cal) = calcite, (Chl) = chlorite, (Dol) = dolomite, (Mag) = magnetite, (Opx) = orthopyroxene, (Spl) = spinel, (Srp) = serpentine, (Tlc) = talc, and (Tr) = tremolite.

alteration haloes around spinel, some of which are altered to magnetite (Fig. 4b). In addition, acicular chlorite was found in patches intergrown with acicular tremolite (Supplementary Fig. S2). Chlorite is also found in the fine-grained material replacing plagioclase (Fig. 5b). Previous studies (Beard et al., 2009; Morishita et al., 2009; Dessimoulie et al., 2020) have found that plagioclase in abyssal samples is replaced by chlorite and either prehnite or hydrogrossular.

Talc (Fig. 4c) is present in seven samples, occurring as either intergrowths or replacements of the tremolite rims on orthopyroxene (Supplementary Fig. S1 and S2). Talc occurs less commonly in the tremolite-filled fractures that cross-cut orthopyroxene, suggesting that talc formed after tremolite. All samples with talc contain chlorite and tremolite. In contrast, four samples (HLY102–85-09, PS59–246-03, PS59–249-12 and PS59–249-60) have small amounts of tremolite present as alteration rims around orthopyroxene, but do not contain either chlorite or talc (Table 1).

Some samples have alteration veins of tremolite ± chlorite ± oxides, in addition to serpentine veins. For example, sample PS59–249-74 (alteration score = 3.5) has a 1 mm wide alteration vein (Fig. 5a) cross-cutting olivine with mesh-texture serpentine and orthopyroxene with talc-tremolite rims. The vein has an interior zone of magnetite, rimmed on both sides by tremolite and then serpentine. The serpentine rim is optically transparent in plane polarized light and contains no magnetite, in contrast to the darker mesh texture serpentine that it cross-cuts (Fig. 5a).

Carbonate veins (Fig. 4d) were found in 11 peridotites (Table 1) as fine-grained carbonate mesh networks (6 samples) or as individual coarse-grained veins (5 samples). In addition, ankerite (Fe-Mg-Mn carbonate) was found in HLY102–85-09 in a complex patch of intergrown alteration minerals (Fig. 5c). The veins always occur as the last generation of alteration, cross-cutting all other alteration. EDS maps indicate that the carbonate mesh networks and individual veins are mixtures of calcite and dolomite (Fig. 4d).

A subset of samples has alteration minerals that occur as brown patches in plane-polarized light (Fig. 5c). They are either intergrown with or cross-cutting other alteration minerals but are too fine-grained for optical identification. In sample HLY102–04-63, we used EDS analysis of a patch replacing olivine to identify mesh texture serpentine filled with olivine, tremolite, corundum, and ankerite (Fig. 5c). Further EDS mapping is needed to determine the systematics of these alteration patches.

One sample, PS59–240-20 (alteration score = 3), has more complex alteration than all other samples (Fig. 6). This sample contains a gabbro vein up to 5 mm thick that consists of plagioclase (Supplementary

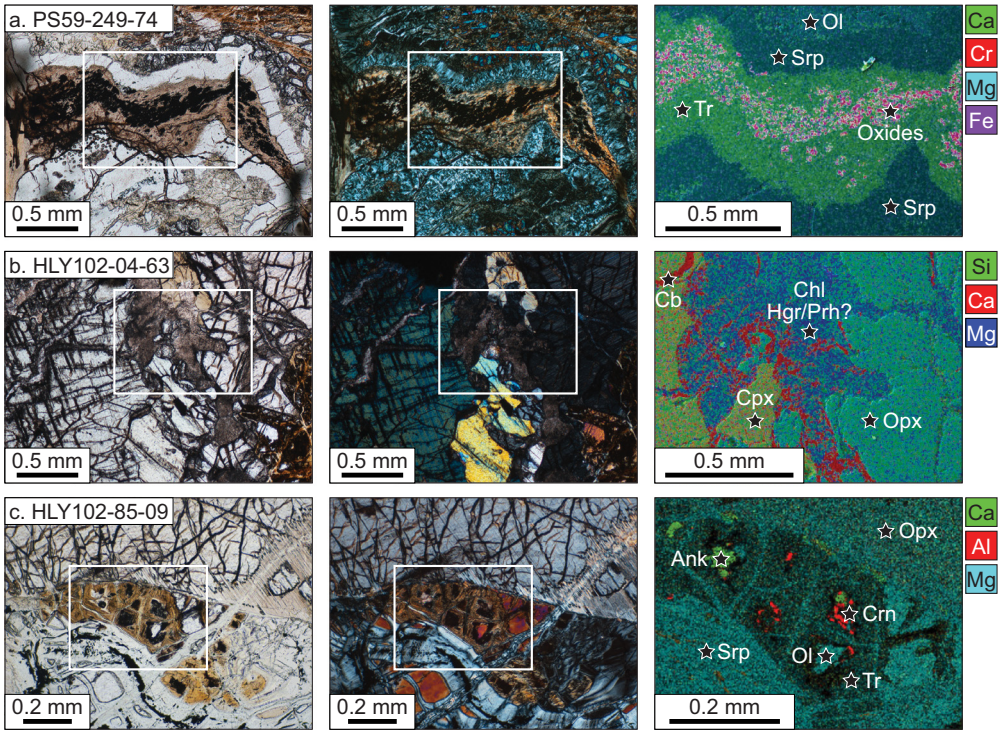


**Fig. 5.** Examples of more complex alteration mineralogy in Gakkel peridotites. Plane-polarized photomicrographs are in column 1, cross-polarized photomicrographs in column 2, and EDS maps in column 3. White boxes indicates the location of the EDS maps. (a) Alteration vein consisting of oxides, tremolite, and serpentine (PS59–249-74). (b) Fine-grained alteration intergrowth replacing plagioclase, likely consisting of chlorite and hydrogrossular or prehnite (HLY102–04-63). (c) Complex alteration patch consisting of mesh texture serpentine filled with a mixture of olivine, tremolite, corundum and ankerite (HLY102–85-09). Mineral abbreviations: (Ank) = ankerite, (Cb) = carbonate, (Chl) = chlorite, (Cpx) = clinopyroxene, (Crn) = corundum, (Hgr) = hydrogrossular, (Ol) = olivine, (Opx) = orthopyroxene, (Prh) = prehnite, (Srp) = serpentine, and (Tr) = tremolite.

Fig. S3), clinopyroxene, magnetite, and ilmenite. A reddish-brown pleochroic amphibole, identified as Ti-rich pargasite by EDS (Fig. 6), replaces some minerals in the vein and in the surrounding peridotite matrix (Supplementary Fig. S3). Coarse-grained tremolite and intergrowths of tremolite needles and talc subsequently replace the pargasite (Fig. 6). Brown serpentine replaces portions of the peridotite matrix, while optically transparent serpentine veins cross-cut all other minerals (Fig. 6c) and a wide serpentine vein truncates one end of the gabbro vein. Parts of the peridotite outside the veins are very fresh and orthopyroxene does not have talc-tremolite rims, though some grains have pargasite crystallized in cross-cutting fractures (Supplementary Fig. S3). The presence of a fine-grained zone that incorporates

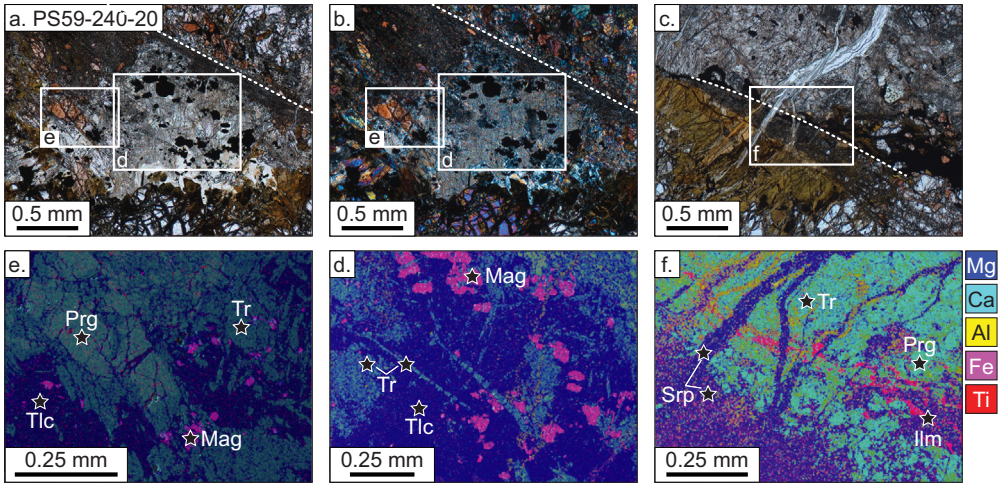


**Fig. 6.** Complexly altered sample PS59–240-20, which is a gabbro-veined lherzolite. (a) Plane-polarized and (b) cross-polarized light photomicrographs of the gabbro vein cross-cutting the sample. The vein has been partially replaced by Ti-rich pargasite (brown pleochroic mineral) and subsequently deformed to produce a fine-grained zone that runs NW-SE across the sample (white dotted line marks upper boundary). Later talc and tremolite overprint the higher-temperature pargasite. (c) Plane-polarized light photomicrograph of another portion of the fine-grained zone (white dotted line marks upper boundary) at the contact between (brown) serpentinized olivine to the southwest and coarse-grained tremolite replacing pargasite to the northeast. A later, optically transparent serpentine vein cross-cuts all other minerals. (e), (d), and (f) show associated EDS maps (white boxes) with mineralogy labeled. Mineral abbreviations: (Ilm) = ilmenite, (Mag) = magnetite, (Prg) = pargasite, (Srp) = serpentine, (Tlc) = talc, and (Tr) = tremolite.

recrystallized pargasite and parts of the gabbro vein, but is overprinted by tremolite and talc (Fig. 6), indicates that the sample underwent high strain ductile deformation after pargasite formation. In addition, olivine and orthopyroxene in the peridotite matrix were partially recrystallized by this deformation.

### 4.3. Whole rock compositions

Whole rock analyses of the Gakkel samples (Supplementary Table S3) confirm that they have a wide compositional range (Fig. 7a). The whole rock $Al_2O_3$ content serves as an indicator of peridotite fertility because $Al_2O_3$ is not mobile during alteration, unlike elements such as $SiO_2$ and MgO (e.g., Malvoisin, 2015; Niu, 1997; Snow and Dick, 1995). The most fertile Gakkel samples contain 3.9 wt% $Al_2O_3$, compared to an estimate of 4 wt% $Al_2O_3$ in the source mantle (Workman and Hart, 2005). Gakkel samples extend to refractory compositions as low as 0.4 wt% $Al_2O_3$ in sample PS59–249-12, in agreement with the absence of clinopyroxene in this sample. The lack of correlation between peridotite alteration score and whole rock $Al_2O_3$ (Fig. 7a) confirms that the overall degree of alteration in a peridotite is independent of the bulk composition. The alteration score also does not correlate with other whole rock major element abundances (Supplementary Fig. S4).

Our application of the alteration scoring system from Birner et al. (2016) demonstrates that the method can be applied to abyssal peridotites from other localities. In Fig. 7b, we show that whole rock LOI is correlated with alteration score for both our Gakkel data and the Tonga data from Birner et al. (2016). As LOI measures the total amount of volatiles present in a sample, it provides a rough proxy for alteration in peridotites, which should have 0 wt% LOI when fresh. While LOI and alteration score are correlated, LOI has a range of ±5 wt% for a given petrographic-based estimate of alteration (Fig. 7b). This likely reflects the heterogeneous distribution of alteration in the peridotite, particularly when alteration minerals are mainly hosted in discrete veins. Despite this scatter, the overall correlation between alteration score and LOI, as well as the correlation of this score with degree of serpentinization (Birner et al., 2016), supports the usefulness of the alteration score as a method for rapidly evaluating alteration in a peridotite.

### 4.4. Pseudosection results

Our pseudosection modeling using Perple_X (Connolly, 2009) indicates that both the nature of chemical reactions and percentage of hydrous phases that form during hydration of abyssal peridotites are highly dependent on peridotite composition and the temperature of fluid-rock interaction (Fig. 8). Our models confirm that serpentine is stable below ~500–600 °C at ridges, in agreement with experimental and natural constraints (Guillot et al., 2015 and references therein). Chlorite crystallizes at <700–800 °C, also in agreement with experiments (Fumagalli and Poli, 2005), and is stable to surface conditions for fertile peridotites. In the pseudosections, tremolite (LT-amphibole) equilibrates between ~570–750 °C in harzburgite and down to lower temperatures in lherzolite. Pargasite (HT-amphibole) equilibrates at temperatures greater than ~700 °C for lherzolite. Talc is stable over a limited temperature range of ~550–650 °C in both harzburgite and lherzolite.

Our models suggest that the volume of amphibole that forms is a function of peridotite fertility (Fig. 8c). Reaction of lherzolite with seawater above 550 °C gives rise to a higher modal percentage of hydrous phases compared to a refractory harzburgite: 24% vs. 5% for tremolite and 16% vs. 3% for chlorite along the P-T path modeled for the Gakkel Ridge (Fig. 8). This indicates that lithosphere dominated by lherzolite has a greater capacity for deep alteration compared to harzburgite. Hydration of more depleted lithologies above 750 °C is not associated with the formation of a hydrous phase. The harzburgite in Fig. 8, which has no clinopyroxene and < 0.5 wt% $Al_2O_3$, produces no HT amphibole, whereas the lherzolite (6% clinopyroxene and 3 wt% $Al_2O_3$) produces 4% HT amphibole.

## 5. Discussion

Our analysis of Gakkel Ridge peridotites reveals variable extents of hydrothermal alteration along the ridge, combined with variations in the alteration mineral assemblages that formed. Below, we evaluate the formation conditions of these different mineral assemblages to better constrain the effects of hydrothermal circulation in an ultramafic-dominated ridge system. We then compare our results to studies from other ridges to evaluate the conditions under which different mineral assemblages form during hydrothermal alteration of the oceanic lithosphere.

### 5.1. Conditions of peridotite alteration along Gakkel Ridge

Gakkel peridotites underwent variable extents of fluid-rock interaction along the 600 km length of ridge that we examined. Peridotites range from unaltered to completely altered with essentially no primary

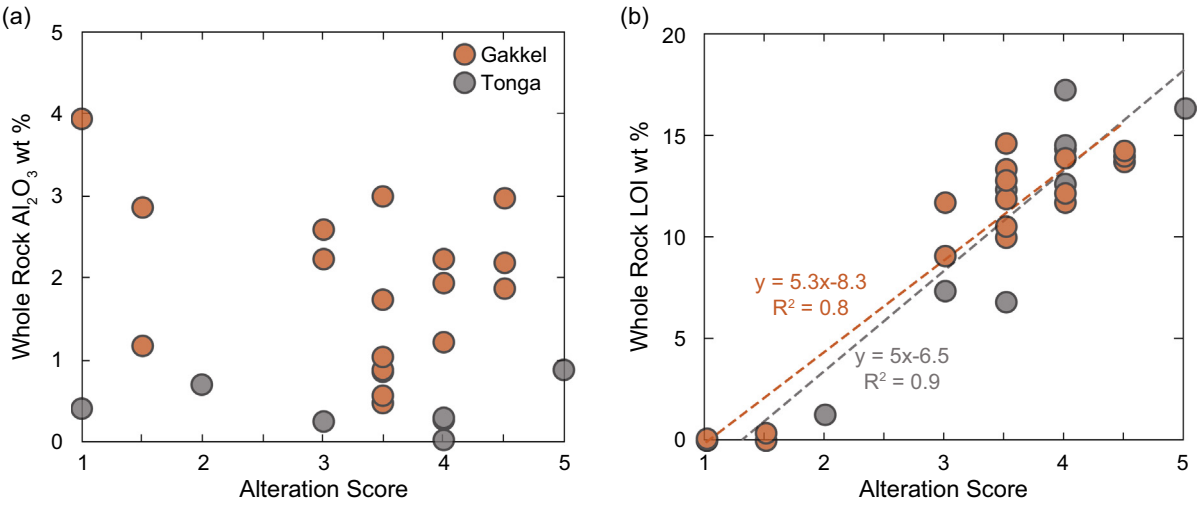


**Fig. 7.** Alteration score versus (a) whole rock $Al_2O_3$ in wt% and (b) Loss on Ignition (LOI) for Gakkel (orange) and Tonga (gray) peridotites. Whole rock compositions are reported in Supplementary Table S3.

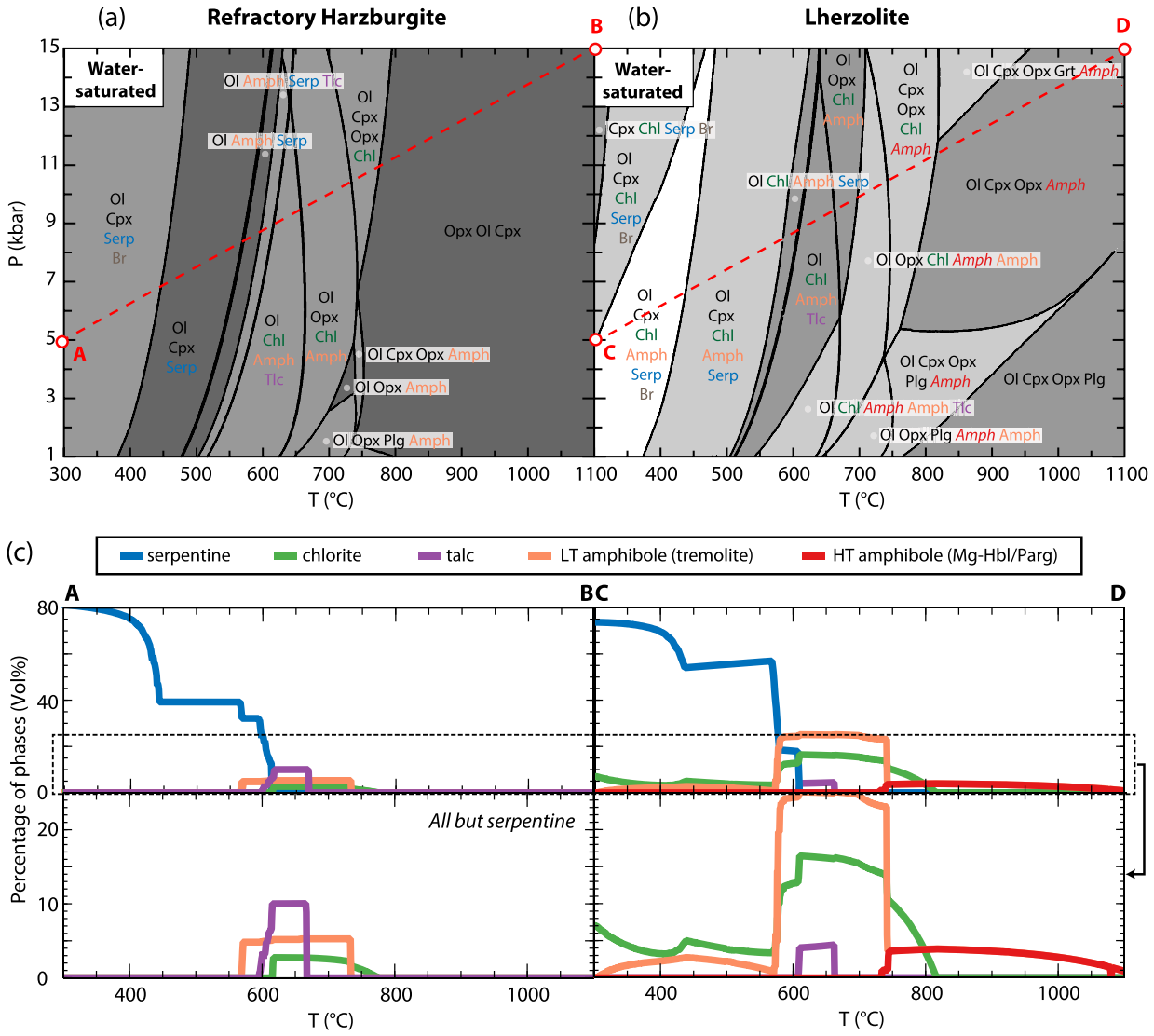


**Fig. 8.** Pseudosections for (a) refractory and (b) fertile peridotites in the NCFMASH system at water-saturated conditions. The calculation for the refractory peridotite uses the whole rock composition of harzburgite BMRG08–98–2-1, which is clinopyroxene-free and has an alteration score of 1. The calculation for the fertile composition uses lherzolite PS59–235-17, which has an alteration score of 1.5. Whole rock compositions are reported in Supplementary Table S3. Red dashed lines show the estimated geotherm for the Gakkel lithosphere. (c) Modal percentage of hydrous phases at thermodynamic equilibrium along the P-T path modeled for the Gakkel Ridge geotherm [profiles A-B on (a) and C-D on (b)].

minerals remaining, with an average alteration score of 3.5 (Fig. 3). Gakkel peridotites with alteration scores >3 were observed along the entire length of the ridge in the study area (Fig. 9). The SMZ is characterized by a wide range of alteration, while EVZ samples have a more limited range, though many fewer peridotite dredges were recovered from this segment. Individual dredges have variations among individual samples up to 4 units on the alteration scale in the SMZ, but only up to 1 in the EVZ. Dredges within 50 km of a vent site have high degrees of alteration, with no samples having scores <3 (Fig. 9). However, vent site regions are under-sampled and details of their effects on peridotite alteration cannot be assessed without higher density sampling of these areas.

Typical alteration minerals in Gakkel peridotites include serpentine, magnetite, tremolite, chlorite, talc, and late-stage carbonates (Table 1). As part of the serpentinization reaction in peridotite, brucite is expected to form (e.g., McCollom and Bach, 2009; Tutolo et al., 2018). The absence of brucite in Gakkel peridotites is either due to brucite reacting out as hydrothermal fluid compositions evolve or due to the low-temperature dissolution of brucite by seawater (e.g., Bach et al., 2004; Klein et al., 2020; Mayhew et al., 2018). Carbonate is present in >25% of samples and is always found as the last generation alteration event. It may have formed in conjunction with brucite dissolution and may have resulted in decreased permeability to fluid flow (Jöns et al., 2017).

The occurrence of the assemblage tremolite + chlorite + talc in a subset of Gakkel samples provides constraints on the temperatures over which hydrothermal alteration occurred. Our pseudosection modeling of lherzolite (Fig. 8b) shows that serpentine + tremolite + chlorite are stable together at ~300-–575 °C for our Gakkel geotherm. This assemblage is followed by tremolite + chlorite + talc at ~600-650 °C for harzburgite and ~575–650 °C for lherzolite (Fig. 8). These models indicate that orthopyroxene in lherzolites initially reacts to form tremolite while clinopyroxene remains stable to higher temperature. This agrees with our observation that orthopyroxene often has rims and fractures filled with tremolite ± talc while clinopyroxene is less often altered to these minerals (Supplementary Fig. S1).

The use of pseudosections to model hydrothermal processes in peridotite applies to the closed-system situation where fluid composition is buffered by the rock during alteration. However, hydrothermal

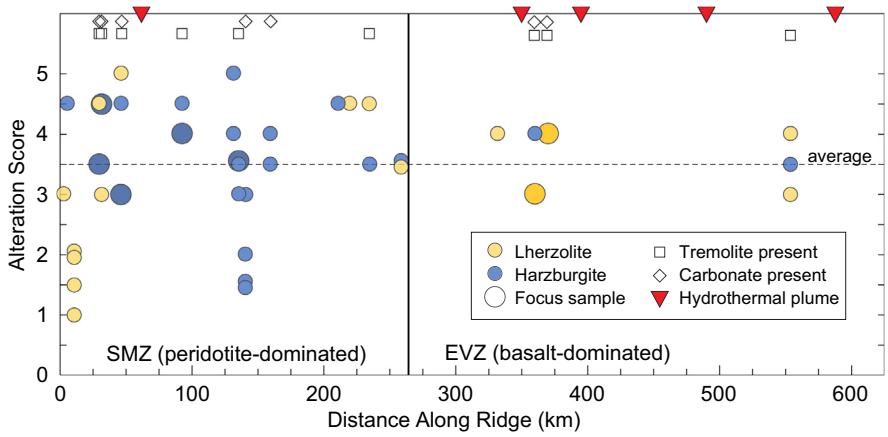


**Fig. 9.** Along-strike variations in the alteration score and lithology of Gakkel peridotites as a function of distance from the WVZ/SMZ boundary at 0 km (see Fig. 1 for geographic locations of boundaries). The black dashed line represents the average alteration score of 3.5. Focus samples analyzed by EDS are indicated by larger circles. Samples with the same alteration score from the same dredge have been slightly offset vertically for visibility. Hydrothermal plume locations, based on coordinates given in Edmonds et al. (2003), are indicated at the top of the figure. Dredges where samples contain tremolite or carbonate (Table 1) are denoted at the top of the figure by squares and diamonds, respectively.

alteration is often an open-system process, particularly when fluids circulate through crustal lithologies in addition to peridotite. For example, Tarling et al. (2018) documented a range of reactions between peridotite and adjacent schist in a serpentinite shear zone. For ridges, the presence of gabbro can help to stabilize tremolite and talc at lower temperatures (e.g., 350 °C–400 °C) by increasing the silica activity of the fluids (Allen and Seyfried, 2003; Bach et al., 2004). However, along the Gakkel Ridge, gabbro corresponds to only 2% of material recovered from the SMZ (Sleep and Warren, 2014), indicating that fluids could not have been modified by the lower crust, as occurs at oceanic core complexes (e.g., Boschi et al., 2006a, 2006b).

Another mechanism that can modify fluid composition is massive fluid circulation through peridotite combined with large-scale dissolution of pyroxenes, which could increase silica and calcium activity sufficiently to stabilize talc and tremolite at lower temperatures. Crystallization of talc, tremolite and chlorite in the rims of orthopyroxene and around spinel suggests that fluid flow was pervasive but localized in close-spaced microfractures during their formation. Similar to serpentine mesh textures (Agrinier and Cannat, 1997; Andreani et al., 2007; Rouméjon et al., 2015; Viti and Mellini, 1998), this argues for relatively low water-rock ratios and equilibration of fluid composition with the peridotite. In contrast, samples with tremolite-serpentine veins (Fig. 5a) and cross-cutting tremolite-chlorite clusters indicate higher water-rock ratios and enhanced fluid flow, which is likely to support a more open system character of alteration.

In our interpretation of closed-system alteration, the occurrence of the assemblage tremolite + chlorite + talc in 20% of our samples suggests that alteration temperatures were sometimes high enough (>500 °C) to stabilize these phases together (Fig. 8). Moreover, the occurence of tremolite in harzburgites also indicates relatively high alteration temperatures (>500 °C; Fig. 8). Our petrographic observations indicate that tremolite typically replaces serpentine, with later formation of talc (Fig. 4). We interpret the serpentine to tremolite to talc sequence to indicate prograde metamorphism with increasing temperature, followed by retrograde formation of cross-cutting veins of tremolite ± chlorite and serpentine. For the prograde metamorphism, fluids must have circulated deep enough in the lithosphere to reach temperatures >500 °C, corresponding to depths >20 km in the SMZ and > 10 km in the EVZ (Schlindwein and Schmid, 2016). Thus, the mineral assemblages in Gakkel samples indicate that hydrothermal fluid temperatures can reach up to 500 °C or higher.

The high degrees of alteration, complex mineral assemblages, and common occurrence of amphibole and talc in Gakkel peridotites (Fig. 9) underscores the prevalence and importance of hydrothermal processes even at ultraslow spreading ridges. This result is surprising given that the lithosphere is colder at ultraslow spreading ridges compared to faster spreading ridges (e.g., Cannat, 1996). However, ship-based observations of the Gakkel Ridge have also noted the abundance of hydrothermal plume sites (Baker et al., 2004; Boetius et al., 2014; Bünz et al., 2020; Edmonds et al., 2003; Helmke et al., 2007; Stranne et al., 2010). Dredges within 50 km of plume sites have high alteration scores (Fig. 9) but several dredges far from any identified sites also have high scores and contain tremolite + chlorite + talc, suggesting that more sites may be present.

### 5.2. Maximal depth of hydrothermal circulation

One sample, PS59–240-20, shows evidence for more complex and higher (>750 °C) temperature alteration compared to all other Gakkel samples. This sample contains a brown pleochroic, Ti-rich amphibole of pargasitic composition similar to that observed in other peridotite massifs (Agrinier et al., 1993; Melson et al., 1972; Roden et al., 1984). Titanium-enrichment has been interpreted to result from amphibole crystallization in peridotite from a hydrous basaltic melt (e.g., Agrinier et al., 1993). However, the gabbro vein in PS59–240-20 appears to predate pargasite formation, as pargasite replaces clinopyroxene and occurs in cross-cutting fractures in orthopyroxene (Supplementary Fig. S3). As the abundance of pargasite in this sample requires a high water content, pargasite crystallization is better explained by hydrothermal fluid flow. As HT amphibole can only crystallize at >750 °C in fertile peridotites (Fig. 8), the presence of pargasite suggests that Gakkel alteration was able to reach temperatures >750 °C in the SMZ, which corresponds to >30 km in this section of the Gakkel Ridge (Schlindwein and Schmid, 2016).

The occurrence of pargasite in one sample, along with the presence of tremolite ± chlorite ± talc in one-third of our samples, provide evidence of deep fluid circulation beneath the Gakkel Ridge. These observations agree with the microseismicity survey of Schlindwein and Schmid (2016), which found that fracturing extends deep into the Gakkel lithosphere and was interpreted to indicate deep fluid flow. The occurrence of deep fluid flow at Gakkel is also consistent with recent petrological observations for the Lanzo peridotite massif, an exhumed ultraslow spreading ridge. Vieira Duarte et al. (2020) observed pargasitic amphibole with high chlorine contents, which indicates seawater hydration of the lithosphere at temperatures up to 800–850 °C.

### 5.3. Comparison of Gakkel peridotite alteration to other ridges

Serpentinization of peridotite has been the subject of many studies (e.g., Barnes and O'Neil, 1969; Coleman, 1971; Seyfried and Dibble,

1980; Ulmer and Trommsdorff, 1995; Fryer et al., 2000; Rouméjon and Cannat, 2014; Cooperdock et al., 2018). However, other alteration minerals in peridotites have received considerably less attention, with most detailed observations of seafloor samples focused on oceanic core complexes. These are sections of lower crust and upper mantle exposed by exhumation along low-angle detachment faults at slow spreading ridges (e.g., Cann et al., 1997a, 1997b; Escartín et al., 2003; Bach et al., 2004; Morishita et al., 2009; Tao et al., 2020). Alteration of ultramafic rocks in these settings results in the formation of talc-tremolite-chlorite schists in the detachment fault zone (e.g., Boschi et al., 2006a, 2006b; Escartín et al., 2003; Picazo et al., 2012; Rouméjon et al., 2018). Formation of these schists is associated with the percolation of seawater through gabbro, which leads to enrichment of the fluids in Si, Ca, and Al (e.g., Boschi et al., 2006a; Picazo et al., 2012, 2013). This leads to the interpretation that talc-amphibole-chlorite schists form by localized fluid flow along the detachment fault, causing open-system alteration of peridotite at <500 °C (Bach et al., 2004; Escartín et al., 2003). In particular, increases in silica and calcium activities in the hydrothermal fluid stabilize talc and tremolite at lower temperatures (Allen and Seyfried, 2003).

The abundances and textures of tremolite, chlorite, and talc assemblages in Gakkel peridotites are substantially different from those in oceanic core complexes. At Gakkel, these minerals form alteration rims and haloes around primary minerals, whereas they occur as massive or foliated schists in the oceanic core complexes. Formation of the schists requires large-scale fluid flow that transfers Ca and Si from the lower crustal gabbro to the peridotite (e.g., Escartín et al., 2003; Boschi et al., 2006a). In contrast, only small amounts of gabbro have been recovered from the Gakkel Ridge, with several sections of the ridge yielding only peridotite (Michael et al., 2003). Geophysical surveys indicate average crustal thicknesses <3 km and the occurrence of discrete volcanic centers (Jokat et al., 2003). Thus, alteration conditions of Gakkel peridotites are different (nearer to closed-system conditions) than the open-system alteration of mafic-ultramafic systems that occurs at oceanic core complexes.

In contrast to the core complexes, the easternmost SWIR at 62–65°E is a similar tectonic environment to that of the Gakkel Ridge, as the spreading rate is also ultraslow (<20 mm/yr) and this part of the ridge is nearly amagmatic, with <3% of dredged samples consisting of basaltic or gabbroic rocks (Sauter et al., 2013). The ultramafic rocks consist predominantly of lherzolite and harzburgite, with partial alteration of pyroxene to tremolite ± chlorite ± talc in a subset of samples (Rouméjon et al., 2015; Dessimoulie et al., 2020). The similarity in the mineral assemblages in SWIR and Gakkel samples suggests similar conditions of hydrothermal alteration in these two settings, both of which lack significant contributions from crustal components.

## 6. Conclusions

Our systematic characterization of alteration in abyssal peridotites from the Gakkel Ridge shows that hydrothermal circulation strongly affects the ultramafic rocks exposed along more than 600 km of this ultraslow-spreading mid-ocean ridge system. Gakkel peridotites span the entire alteration scale, from 1 (nearly pristine) to 5 (completely altered). Alteration scores positively correlate with whole rock LOI, supporting the use of these scores for rapidly evaluating alteration in a peridotite. Reassessment of Tonga peridotite alteration scores in this study also shows that uncertainty related to subjective determination of sample scores is small (±0.5). Alteration scores do not correlate with peridotite lithology or whole rock $Al_2O_3$, indicating that the degree of alteration is not a function of the sample composition.

Tremolite was identified in 33% of Gakkel samples, along with chlorite and talc in a subset of these samples. Cross-cutting carbonate veins occur in 27% of samples. Due to the lack of crust in most of the locations of our peridotite dredges, we modeled peridotite alteration assuming closed-system conditions. Our models suggest that formation of the assemblage tremolite + chlorite + talc requires temperatures >500 °C, while the presence of pargasite in one sample indicates temperatures >750 °C. This implies that hydrothermal fluid circulation occurred in the Gakkel lithosphere to depths >20 km. Our observations of alteration mineral assemblages in peridotites are different to those at oceanic core complexes, in which the presence of gabbro leads to open-system alteration. Instead, the alteration of Gakkel peridotites is similar to alteration in peridotites from the SWIR at 62–65°E, where mafic crust is also not present.

Supplementary data to this article can be found online at https://doi.org/10.1016/j.lithos.2021.106107.

## Funding

This work was supported by the National Science Foundation [OCE-1620276 to J.M.W.], a University of Delaware Summer Fellowship [to S.N.P.], and the University of Delaware Department of Earth Sciences. This work benefited from an American Geophysical Union Student Travel Grant to present an early version of these results [to S.N.P.]

## Declaration of Competing Interest

The authors declare that they have no known competing financial interests or personal relationships that could have appeared to influence the work reported in this paper.

## Acknowledgements

We thank Suzanne Birner, Frieder Klein, and Matthew Tarling for their discussions of this work. We thank the University of Delaware Keck CAMM facility for use of equipment. Finally, we thank Michael Roden for editorial handling and reviewers Matthew Tarling and Benjamin Tutolo for their thoughtful and constructive comments, which helped to improve the manuscript.

## References

Abercrombie, R.E., Ekström, G., 2001. Earthquake slip on oceanic transform faults. Nature 410 (6824), 74–77.

Agrinier, P., Mével, C., Bosch, D., Javoy, M., 1993. Metasomatic hydrous fluids in amphibole peridotites from Zabargad Island (Red Sea). Earth Planet. Sci. Lett. 120, 187–205.

Agrinier, P., Cannat, M., 1997. Oxygen-isotope constraints on serpentinization processes in ultramafic rocks from the Mid- Atlantic Ridge (23°N). In: Karson, J.A., Cannat, M., Miller, D.J., Elthon, D. (Eds.), Proceedings of the Ocean Drilling Program, Scientific Results. 153, pp. 381–388.

Allen, D.E., Seyfried, W.E., 2003. Compositional controls on vent fluids from ultramafic-hosted hydrothermal systems at mid-ocean ridges: an experimental study at 400°C, 500 bars. Geochim. Cosmochim. Acta 67 (8), 1531–1542.

Andreani, M., Mével, C., Boullier, A.-M., Escartin, J., 2007. Dynamic control on serpentine crystallization in veins: constraints on hydration processes in oceanic peridotites. Geochem. Geophys. Geosyst. 8 (2) Q02012.

Bach, W., Garrido, A.J., Paulick, H., Harvey, J., Rosner, M., 2004. Seawater-peridotite interactions: First insights from ODP Leg 209, MAR 15°N. Geochem. Geophys. Geosyst. 5 (9) Q09F26.

Baker, E.T., Edmonds, H.N., Michael, P.J., Bach, W., Dick, H.J.B., Snow, J.E., Walker, S.L., Banerjee, N.R., Langmuir, C.H., 2004. Hydrothermal venting in magma deserts: the ultraslow-spreading Gakkel and Southwest Indian Ridges. Geochem. Geophys. Geosyst. 5-8, 1525–2027.

Barnes, I., O'Neil, J.R., 1969. The relationship between fluids in some fresh alpine-type ultramafics and possible modern serpentinization, Western United States. GSA Bull. 80 (10), 1947–1960. https://doi.org/10.1130/0016-7606(1969)80[1947:TRBFIS]2.0.CO;2.

Beard, J.S., Frost, B.R., Fryer, P., McCaig, A., Searle, R.C., Ildefonse, B., et al., 2009. Onset and progression of serpentinization and magnetite formation in olivine-rich troctolite from IODP hole U1309D. J. Petrol. 50 (3), 387–403.

Birner, S.K., Warren, J.M., Cottrell, E., Davis, F.A., 2016. Hydrothermal alteration of seafloor peridotites does not influence oxygen fugacity recorded by spinel oxybarometry. Geology G38113, 1.

Birner, S.K., Warren, J.M., Cottrell, E., Davis, F.A., Kelley, K.A., Falloon, T.J., 2017. Forearc Peridotites from Tonga Record Heterogeneous Oxidation of the Mantle following Subduction Initiation. J. Petrol. 58 (9), 1755–1780.

Boetius, A., Bach, W., Borowski, C., Diehl, A., German, C., Kaul, N., Köhler, J., Marcon, Y., Mertens, C., Molari, M., Schlindwein, V., Türke, A., Wegener, G., Science Party of RV POLARSTERN Expedition Aurora PS86, 2014. Exploring the Habitability of Ice-Covered Waterworlds: The Deep-Sea Hydrothermal System of the Aurora Mount at Gakkel Ridge, Arctic Ocean (82°54' N, 6°15W, 4000 M) (AGU Fall Meeting).

Boschi, C., Früh-Green, G.L., Delacour, A., Karson, J.A., Kelley, J.S., 2006a. Mass transfer and fluid flow during detachment faulting and development of an oceanic core complex, Atlantis Massif (MAR 30°N). Geochem. Geophys. Geosyst. 7, 1.

Boschi, C., Früh-Green, G.L., Escartín, J., 2006b. Occurrence and significance of serpentinite-hosted, talc-and amphibole-rich fault rocks in modern oceanic settings and ophiolite complexes: an overview. Ofioliti 31, 129–140.

Bünz, S., Ramirez-Llodra, E., German, C., Ferre, B., Sert, F., Kalenickenko, D., Reeves, E., Hand, K., Dahle, H., Kutti, T., Purser, A., Hilario, A., Ramalho, S., Rapp, H.T., Ribeiro, P., Victorero, L., Hoge, U., Panieri, G., Bowen, A., Jakuba, M., Suman, S., Gomez-Ibanez, D., Judge, C., Curran, M., Nalicki, V., Vagenes, S., Lamar, L., Klesh, A., Dessandier, P.A., Steen, I., Mall, A., Vulcano, F., Meckel, E.M., Drake, N., 2020. RV Kronprins Håkon (cruise no. 2019708) Longyearbyen – Longyearbyen 19.09. – 16.10.2019. The Arctic University of Norway.

Cann, J.R., Blackman, D.K., Smith, D.K., McAllister, E., Janssen, B., Mello, S., Avgerinos, E., Pascoe, A.R., Escartín, J., 1997a. Corrugated slip surfaces formed at North Atlantic ridge-transform intersections. Nature 385, 329–332.

Cann, J.R., Blackman, D.K., Smith, D.K., McAllister, E., Janssen, B., Mello, S., Avgerinos, E., Pascoe, A.R., Escartín, J., 1997b. Corrugated slip surfaces formed at North Atlantic ridge-transform intersections. Nature 385, 329–332.

Cannat, M., 1996. How thick is the magmatic crust at slow spreading oceanic ridges. J. Geophys. Res. 101 (B2), 2847–2858.

Connolly, J.A.D., 2009. The geodynamic equation of state: what and how. Geochem. Geophys. Geosyst. 10.

Coleman, R.G., 1971. Petrologic and geophysical nature of serpentinites. Geol. Soc. Am. Bull. 82 (4), 897. https://doi.org/10.1130/0016-7606(1971)82[897:PAGNOS]2.0.CO;2.

Cooperdock, E.H.G., Raia, N.H., Barnes, J.D., Stockli, D.F., Schwarzenbach, E.M., 2018. Tectonic origin of serpentinites on Syros, Greece: Geochemical signatures of abyssal origin preserved in a HP/LT subduction complex. Lithos 296–299, 352–364. https://doi.org/10.1016/j.lithos.2017.10.020.

Craddock, P.R., Warren, J.M., Dauphas, N., 2013. Abyssal peridotites reveal the near-chondritic Fe isotopic composition of the Earth. Earth Planet. Sci. Lett. 365, 63–76.

D'Errico, M.E., Warren, J.M., Godard, M., 2016. Evidence for chemically heterogeneous Arctic mantle beneath the Gakkel Ridge. Geochim. Cosmochim. Acta 174, 291–312.

D'Errico, M.E., Coble, M.A., Warren, J.M., 2019. In situ measurements of lead and other trace elements in abyssal peridotite sulfides. Am. Mineral. 104, 190–206.

DeMets, C., Gordon, R.G., Argus, D.F., Stein, S., 1994. Effect of recent revisions to the geomagnetic reversal time scale on estimates of current plate motions. Geophys. Res. Lett. 21 (20), 2191–2194.

Dessimoulie, L., Delacour, A., Guillame, D., Chevet, J., Cottin, J.-Y., 2020. Major and trace element exchanges during fluid-rock interaction at ultraslow-spreading oceanic lithosphere: example of the South West Indian Ridge (SWIR). Lithos 352-353, 105233.

Edmonds, H.N., Michael, P.J., Baker, E.T., Connelly, D.P., Snow, J.E., Langmuir, C.H., Dick, H.J.B., Mühe, R., German, C.R., Graham, D.W., 2003. Discovery of abundant hydrothermal venting on the ultraslow-spreading Gakkel Ridge in the Arctic Ocean. Nature 421 (January), 252–256.

Engeln, J.F., Wiens, D.A., Stein, S., 1986. Mechanisms and depths of Atlantic transform earthquakes. J. Geophys. Res. 91 (B1), 548–577.

Escartín, J., Mével, C., MacLeod, C.J., McCaig, A.M., 2003. Constraints on deformation conditions and the origin of oceanic detachments: the Mid-Atlantic Ridge core complex at 15° 45'N. Geochem. Geophys. Geosyst. 4 (8), 1067.

Früh-Green, G.L., Kelley, D.S., Karson, J.A., Blackman, D.K., Boschi, C., John, B., Schroeder, T., Ross, D.K., 2001. Hydrothermal Alteration, Serpentinization and Carbonate Precipitation at the lost City Vent Field (30N, Mid-Atlantic Ridge). Am. Geophys. Union T11C–0869.

Früh-Green, G.L., James, A.D., Plas, A., Kelley, D.S., Grobéty, B., 2004. Serpentinization of oceanic peridotites: implications for geochemical cycles and biological activity. Am. Geophys. Union. Geophys. Monogr. Seri. 144, 119–136.

Fryer, P., Lockwood, J.P., Becker, N., Phipps, S., Todd, C.S., 2000. Significance of serpentine mud volcanism in convergent margins. Geological Society of America Special Paper 349, 35–51.

Fumagalli, P., Poli, S., 2005. Experimentally determined phase relations in hydrous peridotites to 6.5 GPa and their consequences on the dynamics of subduction zones. J. Petrol. 46, 555–578.

Fumagalli, P., Zanchetta, S., Poli, S., 2009. Alkali in phlogopite and amphibole and their effects on phase relations in metasomatized peridotites: a high-pressure study. Contrib. Mineral. Petrol. 158, 723–737.

Guillot, S., Schwartz, S., Reynard, B., Agard, P., Prigent, C., 2015. Tectonic significance of serpentinites. Tectonophysics 646, 1–19.

Helmke, E., Juergens, J., Tausendfreund, M., Wollenburg, J., Shank, T., Edmonds, H., Humphris, S., Nakamura, K., Liljebladh, B., Winsor, P., Singh, H., Reeves-Sohn, R.A., 2007. Microbial Communities at Non-Volcanic and Volcanic Sites of the Gakkel Ridge. American Geophysical Union, Fall Meeting 2007 abstract id. OS42A-01.

Jenkins, D.M., 1981. Experimental phase relations of hydrous peridotites modelled in the system H2O-CaO-MgO-Al2O3-SiO2. Contrib. Mineral. Petrol. 77, 166–176.

Johnson, D.M., Hooper, P.R., Conrey, R.M., 1999. GeoAnalytical Lab, Washington State University. Adv. X-ray Analy. 41, 843–867.

Jokat, W., Ritzmann, O., Schmidt-Aursch, M.C., Drachev, S., Gauger, S., Snow, J., 2003. Geophysical evidence for reduced melt production on the Arctic ultraslow Gakkel mid-ocean ridge. Nature 423, 962–965.

Jöns, N., Kahl, W.-A., Bach, W., 2017. Reaction-induced porosity and onset of low-temperature carbonation in abyssal peridotites: Insights from 3D high-resolution microtomography. Lithos 268–271, 274–284.

Kimball, K.L., Spear, F.S., Dick, H.J.B., 1985. High temperature alteration of abyssal ultramafics from the Islas Orcadas Fracture Zone, South Atlantic. Contrib. Mineral. Petrol. 91, 307–320.

Klein, F., Bach, W., Jöns, N., McCollom, T.M., Moskowitz, B., Berquó, T.S., 2009. Iron partitioning and hydrogen generation during serpentinization of abyssal peridotites from 15°N on the Mid-Atlantic Ridge. Geochim. Cosmochim. Acta 73, 6868–6893.

Klein, F., Grozeva, N.G., Seewald, J.S., McCollom, T.M., Humphris, S.E., Moskowitz, B., Kahl, W.A., 2015. Fluids in the Crust. Experimental constraints on fluid-rock reactions during incipient serpentinization of harzburgite. Am. Mineral. 100 (4), 991–1002.

Klein, F., Humphris, S.E., Bach, W., 2020. Brucite formation and dissolution in oceanic serpentinite. Geochem. Perspect. Let. 16, 1–5.

Malvoisin, B., 2015. Mass transfer in the oceanic lithosphere: Serpentinization is not isochemical. Earth Planet. Sci. Lett. 430, 75–85.

Mayhew, L.E., Ellison, E.T., Miller, H.M., Kelemen, P.B., Templeton, A.S., 2018. Iron transformations during low temperature alteration of variably serpentinized rocks from the Samail ophiolite, Oman. Geochim. Cosmochim. Acta 222, 704–728.

McCollom, T.M., Bach, W., 2009. Thermodynamic constraints on hydrogen generation during serpentinization of ultramafic rocks. Geochim. Cosmochim. Acta 73 (3), 856–875.

Melson, W.G., Hart, S.R., Thompson, G., 1972. St. Paul's Rocks, Equatorial Atlantic: Petrogenesis, Radiometric Ages, and implications on sea-floor spreading. Geol Soc Am Mem 132, 241–272.

Michael, P.J., Langmuir, C.H., Dick, H.J.B., Snow, J.E., Goldstein, S.L., Graham, D.W., Lehnert, K., Kurras, G., Jokat, W., Mühe, R., Edmonds, H.N., 2003. Magmatic and amagmatic seafloor generation at the ultraslow-spreading Gakkel ridge, Arctic Ocean. Nature 423 (6943), 956–961.

Morishita, T., Hara, K., Nakamura, K., Sawaguchi, T., Tamura, A., Arai, S., et al., 2009. Igneous, alteration and exhumation processes recorded in abyssal peridotites and related fault rocks from an oceanic core complex along the Central Indian Ridge. J. Petrol. 50, 1299–1325.

Niu, N., 1997. Mantle melting and melt extraction processes beneath ocean ridges: evidence from abyssal peridotites. J. Petrol. 38, 1047–1074.

Picazo, S., Cannat, M., Delacour, A., Escartin, J., Rouméjon, S., Silantyev, S., 2012. Deformation associated with the denudation of mantle-derived rocks at the Mid-Atlantic Ridge 13°-15°N: the role of magmatic injections and hydrothermal alteration. Geochem. Geophys. Geosyst. 13 (9).

Picazo, S., Manatschal, G., Andréani, M., 2013. Deformation associated to exhumation of serpentinized mantle rocks in a fossil Ocean Continent transition: the Totalp unit in SE Switzerland. Lithos 175-176, 255–271.

Prigent, C., Warren, J.M., Kohli, A.H., Teyssier, C., 2020. Fracture-mediated deep seawater flow and mantle hydration on oceanic transform faults. Lithos 532, 115988.

Roden, M.K., Hart, S.R., Frey, A.F., Melson, W.G., 1984. Sr, Nd and Pb isotopic and REE geochemistry of St. Paul's Rocks: the metamorphic and metasomatic development of an alkali basalt mantle source. Contrib. Mineral. Petrol. 85, 376–390.

Rouméjon, S., Cannat, M., 2014. Serpentinization of mantle-derived peridotites at mid-ocean ridges: Mesh texture development in the context of tectonic exhumation. Geochem. Geophys. Geosyst. 15 (6), 2354–2379.

Rouméjon, S., Cannat, M., Agrinier, P., Godard, M., Andreani, M., 2015. Serpentinization and fluid pathways in tectonically exhumed peridotites from the Southwest Indian Ridge (62–65°E). J. Petrol. 56 (4), 703–734.

Rouméjon, S., Früh-Green, G.L., Orcutt, B.N., the IODP Expedition 357 Science Party, 2018. Alteration heterogeneities in peridotites exhumed on the southern wall of the Atlantis Massif (IODP Expedition 357). J. Petrol. 59 (7), 1329–1358.

Ryan, W.B.F., Carbotte, S.M., Coplan, J.O., 2009. Global multi-resolution topography synthesis. Geochem. Geophys. Geosyst. 10, 1–9.

Sauter, D., Cannat, M., Rouméjon, S., Andreani, M., Birot, D., Bronner, A., et al., 2013. Continuous exhumation of mantle-derived rocks at the Southwest Indian Ridge for 11 million years. Nat. Geosci. 6 (4), 314–320.

Schlindwein, V.S.N., Demuth, A., Korger, E., Läderach, C., Schmid, F., 2015. Seismicity of the Arctic mid-ocean Ridge system. Polar Sci. 9 (1), 146–157.

Schlindwein, V., Schmid, F., 2016. Mid-ocean-ridge seismicity reveals extreme types of ocean lithosphere. Nature 535, 276–279.

Schmidt, M.W., Poli, S., 1998. Experimentally based water budgets for dehydrating slabs and consequences for arc magma generation. Earth Planet. Sci. Lett. 163, 361–379.

Seyfried, W.E., Dibble, W.E., 1980. Seawater-peridotite interaction at 300°C and 500 bars: implications for the origin of oceanic serpentinites. Geochim. Cosmochim. Acta 44, 309–321.

Sleep, N.H., Warren, J.M., 2014. Effect of latent heat of freezing on crustal generation at low spreading rates. Geochem. Geophys. Geosyst. 15 (8), 3161–3174.

Snow, J.E., Dick, H.J.B., 1995. Pervasive magnesium loss by marine weathering of peridotite. Geochim. Cosmochim. Acta 59 (20), 4219–4235.

Stranne, C., Sohn, R.A., Liljebladh, B., Nakamura, K., 2010. Analysis and modeling of hydrothermal plume data acquired from the 85°E segment of the Gakkel Ridge. J. Geophys. Res. 115, C06028.

Tao, C., Seyfried, W.E., Lowell, R.P., Liu, Y., Liang, J., Guo, Z., et al., 2020. Deep high-temperature hydrothermal circulation in a detachment faulting system on the ultra-slow spreading ridge. Nat. Commun. 11, 1300.

Tarling, M.S., Smith, S.A.F., Viti, C., Scott, J.M., 2018. Dynamic earthquake rupture preserved in a creeping serpentinite shear zone. Nat. Commun. 1–8.

Tutolo, B.M., Luhmann, A.J., Tosca, N.J., Seyfried, W.E., 2018. Serpentinization as a reactive transport process: the brucite silicification reaction. Earth Planet. Sci. Lett. 484, 385–395.

Ulmer, P., Trommsdorff, V., 1995. Serpentine stability to mantle depths and subduction-related magmatism. Science 268, 858–861.

Vieira Duarte, J.F., Kaczmarek, M.A., Vonlanthen, P., Putlitz, B., Müntener, O., 2020. Hydration of a mantle shear zone beyond serpentine stability: a possible link to microseismicity along ultraslow spreading ridges? J. Geophys. Res. Solid Earth 125 (10) e2020JB019509.

Viti, C., Mellini, M., 1998. Mesh textures and bastites in the Elba retrograde serpentinites. Eur. J. Mineral. 10 (6), 1341–1359.

von der Handt, A., 2008. Deciphering petrological signatures of reactive melt stagnation and cooling in the oceanic mantle underneath ultraslow-spreading ridges. PhD Thesis. Johannes Gutenberg-Universität, Mainz.

Wiens, D.A., Stein, S., 1983. Age dependence of oceanic intraplate seismicity and implications for lithospheric evolution. J. Geophys. Res. 88 (B8), 6455–6468.

Workman, R.K., Hart, S.R., 2005. Major and trace element composition of the depleted MORB mantle (DMM). Earth Planet. Sci. Lett. 231, 53–72.